

# Testing the equivalence principle across the Universe: a model-independent approach with galaxy multi-tracing

Sveva Castello,<sup>1</sup> Ziyang Zheng,<sup>2</sup> Camille Bonvin,<sup>1</sup> and Luca Amendola<sup>2</sup>

<sup>1</sup>*Département de Physique Théorique and Center for Astroparticle Physics,  
Université de Genève, Quai E. Ansermet 24, CH-1211 Genève 4, Switzerland*

<sup>2</sup>*Institut für Theoretische Physik, Universität Heidelberg,  
Philosophenweg 16, 69120, Heidelberg, Germany*

We present a test of the equivalence principle on cosmological scales involving minimal assumptions. Our approach relies on the cross-correlation of two different galaxy populations with large-scale relativistic corrections. We construct a measurable quantity  $E_P$  acting as a null test, i.e. deviating from unity whenever the weak equivalence principle is violated. We provide forecasts with the DESI Bright Galaxy Sample and with the Square Kilometre Array Phase 2 (SKA2). The relativistic corrections can be detected with high significance by both surveys, while  $E_P$  can only be measured by SKA2. We forecast a precision around 10–15% across the redshift range between 0.25 and 0.75.

## Introduction

The advent of increasingly accurate and extended cosmological data allows us to probe fundamental aspects of physics in regimes that have been inaccessible so far. In this Letter, we present a new model-independent approach to test the assumption that all bodies fall in the same way in a gravitational potential, i.e. the weak equivalence principle (EP), a cornerstone of general relativity. Our method allows us to assess whether dark matter is subject to the same unscreened long-range gravitational force as baryons, and also whether additional non-gravitational forces (so-called fifth forces) impact the behavior of dark matter.

The idea of testing fundamental properties of gravity through the clustering of galaxies is not new (see e.g. [1, 2]). However, standard analyses usually focus on specific models beyond general relativity, for instance Horndeski scalar-tensor theories [3], and often rely on known physics at early times and/or a standard background cosmological expansion. Moreover, cosmological tests of gravity generally assume that the EP holds (see e.g. [4]), despite the fact that there is no observational evidence of its validity beyond the Solar System and for the unknown dark matter component.

In this Letter, in contrast, we show that future galaxy surveys can test the EP in a highly model-independent way. We identify a key quantity that can be directly measured with galaxy surveys and that acts as a null test of the EP: a deviation from unity in this parameter clearly signals a breaking of the EP, independently of any model. Three key features of our method allow us to reach this goal: 1) the inclusion of large-scale relativistic corrections; 2) the combination of different tracers of large-scale structure; 3) the parametrization of the power spectrum shape in wavebands, rather than adopting a specific model.

Previous studies have already identified the first two ingredients [5–9]. However, these results rely on a fixed shape of the power spectrum at high redshift (before the acceleration of the Universe started), based on the constraints from the Cosmic Microwave Background (CMB). In this work, we drop this assumption, which allows us to test a much wider range of theories. In particular, we can constrain models of gravity that do

not recover general relativity at high redshift, but also dark matter models with additional interactions (with dark photons, self-interactions or interactions with early dark energy) that may modify the shape of the power spectrum at high redshift. Moreover, the method presented here does not rely on any parameterization of the background evolution of the Universe, nor a known time dependence of the deviations from standard gravity.

## The Euler equation and the equivalence principle

We adopt the perturbed Friedmann metric in the Newtonian gauge,  $ds^2 = a^2[-(1+2\Psi)d\tau^2 + (1-2\Phi)d\mathbf{x}^2]$ , with  $\tau$  being the conformal time and  $a$  the scale factor. At late times, the Universe can then be described with four quantities encoding linear perturbations: the matter density fluctuation  $\delta_m$ , the matter velocity field  $\mathbf{V}$  and the two gravitational potentials  $\Phi$  and  $\Psi$ , denoting the spatial and temporal distortions in the space-time geometry. The relations among these quantities are uniquely determined by the theory of gravity and the energy content of the Universe.

The EP is encoded in the Euler equation, relating the velocity  $\mathbf{V}$  and the temporal distortion  $\Psi$ . In general, this equation in Fourier space takes the form [5, 10]

$$V' + [1 + \Theta(k, z)]V - \frac{k}{\mathcal{H}}[1 + \Gamma(k, z)]\Psi = 0, \quad (1)$$

where a prime denotes a derivative with respect to  $\ln a$ ,  $\mathcal{H}$  is the Hubble parameter in conformal time, and  $V$  is the velocity potential in Fourier space, defined through  $\mathbf{V} = i\mathbf{k}V/k$ . The quantities  $\Theta$  and  $\Gamma$  are free functions of scale and redshift, which respectively encode a friction term and a fifth force acting on dark matter. Both of them vanish if the equivalence principle is respected. As shown in [5], this formulation covers a rich phenomenology, including scenarios where dark matter is non-minimally coupled to an additional scalar or vector field. As an example, the expressions for these functions in a coupled dark energy model can be found in [10] and for Horndeski theories in [11].

Our objective is to develop a test indicating whether the functions  $\Theta$  and  $\Gamma$  take a nonzero value in our Universe. In the spirit of being fully model-independent, we

also allow for generic deviations from standard gravity encoded in a function  $\mu_G$  in the Poisson equation,

$$\Psi = -\frac{3}{2}\mu_G(k, z) \left(\frac{\mathcal{H}}{k}\right)^2 \Omega_m \delta_m, \quad (2)$$

where  $\Omega_m(z)$  is the matter density parameter at redshift  $z$ . Models where dark matter is subject to additional non-gravitational forces have  $\mu_G = 1$ , whereas modified gravity theories with a different coupling to dark matter and baryons typically have  $\mu_G \neq 1$ .

As we shall see, the distribution of galaxies provides direct measurements of the quantity

$$E_P \equiv 1 + \Theta - \frac{3\Omega_m\mu_G\Gamma}{2f}, \quad (3)$$

where  $f \equiv \delta'_m/\delta_m$  is the growth rate of cosmic structure. The parameter  $E_P$  provides a robust criterion to test the EP since it deviates from unity whenever the Euler equation is not valid, independently of the physical origin of this violation. More precisely, if gravity is not modified ( $\mu_G = 1$ ) but an additional non-gravitational force acts on dark matter, we have  $E_P \neq 1$ . If gravity couples differently to dark matter and baryons ( $\Theta, \Gamma \neq 0$  and possibly  $\mu_G \neq 1$ ),  $E_P$  also deviates from unity. On the other hand, if gravity is modified in a way that respects the EP, then  $E_P = 1$ .

A physical interpretation of  $E_P$  can be obtained considering a simple model with a constant dark matter-dark energy coupling  $\hat{\beta}$  and  $\mu_G = 1$  [12]. In this case, we have  $E_P = 1 + c_1\hat{\beta} + c_2\hat{\beta}^2$ , with  $c_{1,2}$  of order unity today. Therefore,  $E_P$  deviates from unity proportionally to the strength of the EP-violating interaction. We also note that  $E_P$  can be linked to the function  $E^{\text{break}}$  defined in Eq. (4.1) in [6] by relating velocities and gravitational potential to the density field. In the following, we forecast constraints on  $E_P$  from galaxy surveys.

### A model-independent test from galaxy clustering

Galaxy surveys measure the galaxy number counts fluctuations,

$$\Delta(\hat{\mathbf{n}}, z) \equiv [N(\hat{\mathbf{n}}, z) - \bar{N}(z)]/\bar{N}(z), \quad (4)$$

where  $N$  is the number of galaxies per pixel detected in direction  $\hat{\mathbf{n}}$  and at redshift  $z$ , and  $\bar{N}$  denotes the average number per pixel. In the linear regime, the observable  $\Delta$  is given by [13–15]

$$\begin{aligned} \Delta(\hat{\mathbf{n}}, z) &= b_g \delta_m - \frac{1}{\mathcal{H}} \partial_r (\mathbf{V} \cdot \hat{\mathbf{n}}) \\ &+ \frac{1}{\mathcal{H}} \partial_r \Psi + \mathbf{V}' \cdot \hat{\mathbf{n}} + \alpha \mathbf{V} \cdot \hat{\mathbf{n}}, \end{aligned} \quad (5)$$

where  $r$  is the comoving distance,  $b$  is the galaxy bias and we have defined

$$\alpha \equiv 1 - 5s + \frac{5s - 2}{\mathcal{H}r} - \frac{\mathcal{H}'}{\mathcal{H}} + f^{\text{evol}}. \quad (6)$$

Here,  $s$  is the magnification bias, accounting for the fact that surveys are flux limited, and  $f^{\text{evol}}$  is the evolution bias, encoding the evolution of galaxies.

The first line of Eq. (5) contains the density contribution and the well-known redshift-space distortions (RSD), accounting for the impact of the galaxy velocities on the redshift [16]. These terms have been used to test gravity in clustering analyses, see e.g. [17]. The terms in the second line of (5) are relativistic corrections, suppressed in Fourier space by one power  $\mathcal{H}/k$  with respect to density and RSD. These corrections involve Doppler contributions proportional to  $\mathbf{V}$  and  $\mathbf{V}'$  and the gravitational redshift effect proportional to  $\Psi$ . We will see that the relativistic terms, in particular gravitational redshift, provide key information to test the EP.

The quantity  $\Delta$  contains additional relativistic corrections suppressed by  $(\mathcal{H}/k)^2$ . In the following, we choose to work in a regime where these are negligible, imposing cuts in  $k$ , to simplify the modeling of the signal. This does not remove information on the EP since the terms in Eq. (5) already contain  $\Psi$  and  $\mathbf{V}$ , which are the only two relevant quantities to test the EP. By removing low  $k$ -modes we only have a marginal loss of constraining power, since these modes are strongly affected by cosmic variance.<sup>1</sup>

As usual in this kind of analysis, we assume that the non-linear gravitational coupling between dark matter halos and their galaxy content does not generate a sizeable velocity bias (even in presence of an EP violation), so that we equate the galaxy velocity with the dark matter velocity. We also neglect the contribution to the galaxy velocity due to the baryons (obeying the EP), as this was shown to have a negligible impact [7].

In Fourier space Eq. (5) takes the form

$$\Delta(\mathbf{k}, \hat{\mathbf{n}}, z) = b_g \delta_m - \frac{\mu^2}{\lambda} V - i \frac{\mu}{\lambda} \Psi + i \mu V' + \alpha i \mu V, \quad (7)$$

where  $\lambda \equiv \mathcal{H}/k$  and  $\mu \equiv \hat{\mathbf{k}} \cdot \hat{\mathbf{n}}$ . The relativistic corrections in Eq. (7) break the symmetry of two-point correlations. In order to measure the anti-symmetric contributions, it is necessary to correlate differently biased populations of galaxies, for example a bright (B) and a faint (F) one [21, 22]. Using Euler equation (1) and Poisson equation (2), together with the continuity equation  $V = -\lambda f \delta_m$ , we can rewrite  $\Delta_B$  and  $\Delta_F$  in terms of  $\delta_m$ . We find

$$\Delta_{B,F} = \delta_m b_{B,F} (1 + \beta_{B,F} \mu^2 - i \beta_{B,F} \mu \lambda \gamma_{B,F}), \quad (8)$$

where  $\beta_{B,F} = f/b_{B,F}$  and

$$\gamma_{B,F} \equiv \alpha_{B,F} - E_P. \quad (9)$$

From Eq. (8), we see that the sensitivity to  $E_P$  specifically arises from the relativistic corrections.

In the following, we assume that the bias and growth function do not depend on scale in the linear  $k$ -range

---

<sup>1</sup>  $\Delta$  also contains some integrated contributions such as gravitational lensing, which were shown to be negligible in the low redshift regime ( $z < 1$ ) relevant for this work [18–20].

we consider here. Similarly, although in principle  $E_P$  can depend on scale and time, we only consider its time dependence. This is a good approximation for many models [5], including modified gravity [23], but can be lifted if the data provide enough constraining power.

We now compute the auto- and cross-power spectra  $P_{\Delta_L \Delta_M} \equiv \langle \Delta_L \Delta_M^* \rangle$  (with  $L, M = \{B, F\}$ ), keeping terms only up to order  $\lambda$ :

$$P_{\Delta_F \Delta_F} = (1 + \beta_F \mu^2)^2 \frac{\beta_B}{\beta_F} S_g^2 B P, \quad (10)$$

$$P_{\Delta_B \Delta_B} = (1 + \beta_B \mu^2)^2 \frac{\beta_F}{\beta_B} S_g^2 B P, \quad (11)$$

$$P_{\Delta_F \Delta_B} = [(1 + \beta_F \mu^2)(1 + \beta_B \mu^2) + i\lambda\mu(\tau_1 + \mu^2\tau_2)] S_g^2 B P, \quad (12)$$

where  $P$  is the power spectrum at  $z = 0$  and  $B \equiv b_B b_F G(z)^2$ , with the linear growth factor  $G \equiv \delta_m(z)/\delta_m(0)$ . The quantity  $S_g(k, \mu, z)$  is a damping factor encoding corrections due to non-linear RSD and spectroscopic errors. The parameters  $\tau_1$  and  $\tau_2$  appearing in the cross-spectrum are given by

$$\tau_1 = \beta_B \alpha_B - \beta_F \alpha_F - E_P(\beta_B - \beta_F), \quad (13)$$

$$\tau_2 = \beta_B \beta_F (\alpha_B - \alpha_F). \quad (14)$$

The expression for  $\tau_1$  clearly shows that  $E_P$  can be measured only if  $\beta_B \neq \beta_F$ , hence requiring two differently biased populations of galaxies. We also note that  $\alpha_{B,F}$  only depends on measurable quantities, i.e. background terms and  $s_{B,F}, f_{B,F}^{\text{evol}}$ , which can be measured from the mean distribution of galaxies. Hence, the spectra in Eqs. (10)-(12) are only functions of  $B(z), \sigma_g(z), \beta_{B,F}(z), E_P(z)$  and  $P(k)$ , where  $\sigma_g(z)$  encodes the non-linear velocity dispersion entering in  $S_g$ , see Eq. (20).

As discussed in [22], the correlations are affected by wide-angle corrections from RSD, due the fact that the line of sight to two correlated galaxies are not parallel. These terms are of the same order as the relativistic corrections and hence cannot be neglected. We calculate them following [24], but using the middle-point configuration for the correlations, where  $\mu$  is the cosine angle between the vector  $\hat{\mathbf{k}}$  and the direction to the mean point in the separation between the galaxies. With this, we find

$$P_{\Delta_F \Delta_B}^{\text{wa}} = -\frac{2}{5} \frac{1}{\mathcal{H}r} (\beta_F - \beta_B) i\lambda B P \times \left( 5\mu^3 - \frac{5}{2}\mu(\mu^2 - 1) \frac{d \log P}{d \log k} \right), \quad (15)$$

to be added to Eq. (12). This contribution scales with  $\lambda$  and is therefore of the same order as the relativistic terms in the cross-spectra. Wide-angle corrections on the auto-spectra are instead of order  $\lambda^2$ , thus negligible with respect to density and RSD.

### Fisher analysis

Following the methodology of [25], we build the data covariance matrix for each bin in wavenumber  $k = |\mathbf{k}|$

and cosine angle  $\mu$  as

$$C = \begin{pmatrix} P_{\Delta_F \Delta_F} + P_{\text{sn}, \Delta_F} & P_{\Delta_F \Delta_B} \\ P_{\Delta_B \Delta_F} & P_{\Delta_B \Delta_B} + P_{\text{sn}, \Delta_B} \end{pmatrix} \quad (16)$$

Here, the shot noise terms are  $P_{\text{sn}, \Delta_{B,F}} = n_{B,F}^{-1}$ , where  $n_{B,F}$  are the galaxy number densities. Since

$$P_{\Delta_F \Delta_B} = \langle \Delta_F \Delta_B^* \rangle = \langle \Delta_F^* \Delta_B \rangle^* = P_{\Delta_F \Delta_B}^*, \quad (17)$$

the covariance matrix is Hermitian. The Fisher Matrix (FM) for the  $n$ -th  $k$  bin and the  $m$ -th  $\mu$  bin is the trace of products of commuting Hermitian matrices and is therefore real,

$$F_{\alpha\beta}^{nm} = \frac{1}{2} \frac{\partial C_{ij}}{\partial \theta_\alpha} C_{jp}^{-1} \frac{\partial C_{pq}}{\partial \theta_\beta} C_{qi}^{-1}, \quad (18)$$

where  $\theta_\alpha$  is the parameter vector. The total FM, summed over the  $k, \mu$  bins, reads

$$F_{\alpha\beta, \text{tot}} = \frac{V}{8\pi^2} \sum_{n,m} k_n^2 \Delta k_n \Delta \mu_m F_{\alpha\beta}^{nm}. \quad (19)$$

We choose a constant  $\Delta \mu_m = 0.1$  and  $\Delta k_n = 0.01 h/\text{Mpc}$ . The spectra are multiplied by factors that take into account the Finger-of-God (FoG) effect and the spectroscopic errors (see e.g. [26, 27]):

$$S_g(k, \mu, z) = \exp[-(k\mu\sigma_z)^2/2] \exp[-(k\mu\sigma_g)^2/2], \quad (20)$$

where  $\sigma_z = \sigma_0(1+z)H(z)^{-1}$ . We take  $\sigma_0 = 0.001$  for the spectroscopic errors and leave the damping strengths  $\sigma_g$  as free parameters in each bin.

To convert redshifts and angles to Fourier wavevectors, one needs an arbitrary reference cosmology, which we denote with the subscript  $r$ . In any other cosmology,  $k$  and  $\mu$  are distorted by the Alcock-Paczynski (AP) effect, so that  $\mu = \mu_r h/\alpha_{\text{AP}}$  and  $k = \alpha_{\text{AP}} k_r$ , where [28]

$$\alpha_{\text{AP}} = \frac{1}{d} \sqrt{\mu_r^2 (h^2 d^2 - 1) + 1}. \quad (21)$$

The distortion therefore depends on  $h \equiv E/E_r$  and on  $d \equiv L_A/L_{Ar}$ , where  $E(z) \equiv H(z)/H_0$  is the dimensionless Hubble function and  $L_A(z) \equiv H_0 D_A(z)$  is the dimensionless comoving angular diameter distance. Since  $d$  is degenerate with the power spectrum at the linear level, we will consider the combination  $h_d \equiv hd$  as a parameter in our analysis. This combination, up to a normalization, is often denoted as  $F_{\text{AP}}$  (see e.g. [29]). We also note that the product  $\mathcal{H}r$  appearing in Eq. (15) can be written in terms of our parameters as  $E_r L_{Ar} h_d$ .

To summarize, the set of free parameters in each  $z$ -bin is  $\{h_d, d, B, \sigma_g, \beta_B, \beta_F, E_P\}$ . In addition, we parametrize the power spectrum shape in several wavebands in the first redshift bin  $z_1$  and evolve it with the free function  $B(z)$ . We take the  $k$ -range  $k \in (0.01 - 0.12) h/\text{Mpc}$  with intervals  $\Delta k = 0.01 h/\text{Mpc}$ , for a total of twelve  $P(k)$  waveband parameters and seven  $z$ -dependent parameters per  $z$ -bin.

We adopt uniform infinite priors (i.e. no prior in the Fisher formalism) for all parameters except  $d$ . For the

latter, we adopt a 3% error prior, since already with current data  $d$  can be determined through the Hubble diagram to this level or better when averaged over a redshift bin (e.g. with the Pantheon+ supernova catalog [30]). We fix  $B(z_1)$  to unity in the first bin, as this quantity is fully degenerate with  $P(k, z_1)$ . Hence,  $B(z)$  encodes the ratio  $b_B b_F G^2$  with respect the first bin.

The last term in Eq. (15) introduces a significant complication as it contains a derivative, and hence it needs to be evaluated taking finite differences among  $k$  bins. However, we find that the entire wide-angle correction is sub-dominant in the  $k, z$  range we explore, and the derivative term itself only changes the constraints on  $E_P$  by less than 4%. For this reason, we fix the derivative term to the fiducial value. A similar problem arises with the derivative term  $\mathcal{H}'/\mathcal{H}$  in Eq. 6. Here too we find that neglecting this term changes the main constraints by at most 5% within each bin, such that we can safely fix  $\mathcal{H}'/\mathcal{H}$  to its fiducial value. Note that this procedure can be iterated when working with data: after obtaining constraints on  $h$  and  $P(k)$ , we can re-calculate  $dP/dk$  and  $\mathcal{H}'/\mathcal{H}$  at the best fit and redo the analysis with this new fiducial, until convergence is reached.

We also apply scale cuts in each redshift bin based on the requirement that the  $\lambda$  hierarchies are preserved, meaning that the terms of order  $\lambda^0$  must be much larger than those of order  $\lambda^1$ , to avoid interference from higher-order terms. In practice, this condition means that we only consider the bins for which the Fisher matrix is positive-definite, which excludes a few low- $k$  bins at each redshift. These conditions ensure that our results remain both physically meaningful and numerically robust.

### Survey specifications and fiducial values

We separately perform the analysis for two surveys: SKA2 [31] and the DESI Bright Galaxy Sample (BGS) [32] (see the Supplemental Material for more information). In both cases, we split the galaxy sample into a bright and a faint population with a redshift-dependent flux cut, chosen such that the two populations have the same number of galaxies in each redshift bin.

We assume a baseline galaxy bias difference  $\Delta b = 1$  between the two populations, based on measurements performed in BOSS [33]. Thus, we choose as fiducial values for the biases  $b_{B,F}(z) = b_g(z) \pm 0.5$ , where  $b_g(z)$  denotes the bias of the total galaxy population. Note that neither  $b_g(z)$  nor  $\Delta b$  are measurable quantities, and that the two free parameters encoding the biases in our analysis are instead  $\beta_B$  and  $\beta_F$ , which we vary around their fiducial values. Since  $E_P$  in Eq. (13) scales with the bias difference, but there are currently no predictions for the expected value of this difference in SKA2 and DESI, we adopt a set of toy models with  $b_{B,F}(z) = b_g(z) \pm 0.3, 0.6$  to study how the constraints on  $E_P$  change. In practice, the bias difference can be boosted through density-based splits of galaxies depending on their environment [34].

Both the magnification and the evolution bias will be directly measurable from the average number of galaxies once the data become available. For the purpose of our

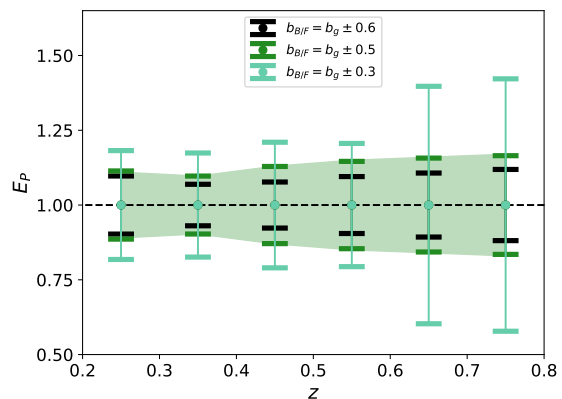


Figure 1. SKA2  $1\sigma$  relative error for  $E_P$  as a function of redshift, for various bias schemes. The black dashed line represents the fiducial value  $E_P = 1$ , while the green shaded region indicates the constraints for the baseline survey.

Table I. DESI relative errors for the baseline bias scheme.

$z$	$\beta_F$	$\beta_B$	$h_d$	$E_P$	$\tau_1$	$B$	$\sigma_g$
0.05	0.064	0.059	0.069	5.1	0.057	-	0.9
0.15	0.042	0.038	0.046	3.3	0.080	0.09	0.42
0.25	0.053	0.048	0.043	4.8	0.14	0.086	0.33
0.35	0.081	0.074	0.042	8.0	0.25	0.085	0.31
0.45	0.16	0.14	0.062	25	0.72	0.092	0.42

analysis, we fix the magnification bias  $s_{B,F}(z)$  according to Appendix B in [7] and the evolution bias  $f^{\text{evol}}$  to 0, as this was shown to have a subdominant impact on the results [11, 33]. For the cosmological parameters  $P(k), d, h_d, B$  and the growth rate  $f$ , we adopt  $\Lambda$ CDM values from the final *Planck* data release [35], while we take a fiducial value of 4.24 Mpc/h for the velocity dispersion  $\sigma_g$  in each redshift bin [27]. Finally, we assume no EP violation as fiducial, i.e.  $E_P = 1$ .

### Results and conclusions

In Table I, we show the relative uncertainties forecasted for DESI with the baseline bias scheme with  $\Delta b = 1$ . To assess whether the relativistic corrections can be detected at all, we can estimate how well we can measure the  $\tau_1$  coefficient in Eq. (12), which encodes the dominant relativistic contribution proportional to  $\mu$  in the cross power spectrum  $P_{\Delta_F \Delta_B}$ . The quantity

Table II. SKA2 relative errors for the baseline bias scheme.

$z$	$\beta_F$	$\beta_B$	$h_d$	$E_P$	$\tau_1$	$B$	$\sigma_g$
0.25	0.0031	0.0015	0.0021	0.11	0.0081	-	0.15
0.35	0.0024	0.0014	0.002	0.097	0.0093	0.035	0.12
0.45	0.0024	0.0016	0.0023	0.13	0.015	0.034	0.096
0.55	0.0026	0.0019	0.0027	0.15	0.020	0.033	0.084
0.65	0.003	0.0023	0.0033	0.16	0.024	0.032	0.077
0.75	0.0035	0.0028	0.004	0.17	0.028	0.032	0.073

$\tau_1$  is not part of our set of parameters, but we can replace  $E_P$  by  $\tau_1$  using Eq. (13). As we see from Table I, DESI can constrain  $\tau_1$  to within 5.7% in the first bin, implying a signal-to-noise ratio of  $1/0.057 \sim 17$ . The constraints degrade for increasing redshift, but they are still robust, except in the last redshift bin. Hence, we conclude that relativistic corrections are expected to be well detected with DESI, in agreement with the results in [33].

However, we find that DESI is unable to constrain  $E_P$  to an acceptable level. Alternative ways of splitting galaxies, like density splits [34] can in principle boost the bias difference, improving the constraints. For example, adopting a quite extreme bias difference of 2.6, we can constrain  $E_P$  to within 40% at  $z = 0.15$ .

For SKA2, we find that the relativistic corrections encoded in  $\tau_1$  can be detected with a precision ranging between 0.8 – 3%, see Table II. Moreover, the  $E_P$  parameter can be constrained to within 10 – 17% in all redshift bins from 0.25 to 0.75, thanks to the larger volume, higher galaxy densities, and larger difference  $\beta_B - \beta_F$  with respect to DESI.

To assess the robustness of the constraints, we have explored different configurations. Notably, we obtain that the relative error on  $E_P$  changes by less than 2% when adopting a lower  $k_{\max} = 0.1 h/\text{Mpc}$ . Moreover, as expected from Eq. (13), we find that the uncertainty on  $E_P$  crucially depends on the bias scheme. In general, the best results are obtained by splitting the galaxy sample into populations with as much of a large  $\Delta\beta$  as possible. For instance, adopting the alternative bias schemes  $b_{B,F} = b_g \pm 0.3$  and  $b_{B,F} = b_g \pm 0.6$ , we obtain weaker or stronger constraints, respectively, as can be seen from Fig. 1. In addition, we find that the constraining power increases when the mean bias  $b_g$  decreases. All our results are prior-independent, except for  $d$ , for which we adopted a data-motivated prior of 3%. Even increasing the prior to 6%, the final errors on  $E_P$  for SKA2 do not change by more than a few percents.

We find that the inclusion of the wide-angle correction helps improving the errors. The effect is small at high redshifts ( $z > 0.35$ ), with the constraint on  $E_P$  improving by at most 10%, but it reaches up to 40% at  $z = 0.25$ . This is due to the fact that the wide-angle correction depends on the combination  $\Delta\beta$ , which is the same factor multiplying  $E_P$ . Therefore, improved constraints from the wide-angle terms help constraining  $E_P$ , also due to the  $\mu$  terms carrying the AP effect and the further dependence on  $P(k)$  in (15).

Concerning the other parameters, we find that the quantities  $h_d, \beta_{B,F}$ , which enter the spectra already at order  $\lambda^0$ , can be measured to within 0.1 – 0.3% with SKA2. The amplitude  $B$  and the linear power spectrum, instead, can be measured to within roughly 3 – 4%. Some of these results are presented in a corner plot in the Supplemental Material.

In conclusion, this work demonstrates that it is possible to measure potential violations of the Equivalence Principle on cosmological scales independently of specific models for the power spectrum shape, the background expansion, the growth rate, and the bias.

## ACKNOWLEDGEMENTS

We are grateful to Enea Di Dio for discussions on the wide-angle terms. SC and CB acknowledge support from the European Research Council (ERC) under the European Union’s Horizon 2020 research and innovation program (grant agreement No. 863929; project title “Testing the law of gravity with novel large-scale structure observables”). LA and ZZ acknowledge support from Deutsche Forschungsgemeinschaft (DFG, German Research Foundation) project 456622116 and from DFG Germany’s Excellence Strategy EXC 2181/1 - 390900948 (the Heidelberg STRUCTURES Excellence Cluster). ZZ thanks the Heidelberg STRUCTURES Excellence Cluster for financially supporting her research visits to Geneva, and the University of Geneva for hospitality. SC is grateful for the hospitality at the Heidelberg University. The Mathematica code we employed to produce the Fisher matrix results is available at [github.com/itpamendola/ep-testing](https://github.com/itpamendola/ep-testing).

## SUPPLEMENTAL MATERIAL

We present the specifications for the DESI and SKA2 surveys used in our forecasts, and the resulting fiducial values for the parameters of the analysis. As specified in the main text, we choose  $\Lambda$ CDM with values from the final *Planck* data release [35]. Note that the observables do not depend on the value of the Hubble constant, which is just a dimensional factor in the units.

**DESI Bright Galaxy Sample.** The survey specifications are given in Table 2.5 in [32]. We compute the galaxy bias from the requirement  $b_g^{\text{BGS}}G(z) = 1.34$  given in Sec. 2.4.2 in [32], where the growth factor  $G(z)$  is normalized at present time and calculated on our fiducial model. The magnification bias of the total galaxy sample is calculated following the specifications from [33]. We again perform a flux cut requiring the same number of galaxies in each sample. We present all specifications in Table III.

**SKA Phase 2.** The survey specifications are given in Table 3 in [31]. The fiducial values for the galaxy bias were obtained with a fitting function for the SKA HI galaxy surveys based on [36]. We compute the fiducial values of the magnification bias of the total galaxy population according to the fitting formula in Appendix A in [37], assuming a flux sensitivity limit of  $5 \mu\text{Jy}$ . We then perform a flux cut as a function of redshift to split the total sample into two populations with the same number of galaxies. We present all specifications in Table IV.

For completeness, we also show in Fig. 2 the corner plot for all parameters at a representative redshift  $z = 0.35$ , and in Fig. 3 the fiducial spectrum at  $z = 0$  with the forecasted errors.

Table III. DESI BGS survey specifications. Here and in the next table, the galaxy densities  $n_g$  are multiplied by  $10^3$  and expressed in units of  $(h/\text{Mpc})^3$  with  $h = 0.67$ ; the volume  $V$  is in  $(\text{Gpc}/h)^3$ .

$z$	$V$	$n_g$	$b_g$	$s_B$	$s_F$	$\beta_B$	$\beta_F$	$\alpha_B$	$\alpha_F$	$\tau_1$	$B$
0.05	0.04	40.8	1.38	0.239	-0.071	0.297	0.634	-17.4	-48.	25.6	1.
0.15	0.23	18.7	1.45	0.479	-0.132	0.314	0.645	1.13	-18.4	12.5	1.01
0.25	0.58	4.61	1.53	0.82	-0.174	0.326	0.642	6.42	-11.8	10.	1.02
0.35	1.04	0.99	1.61	1.34	-0.205	0.334	0.635	10.5	-8.76	9.37	1.03
0.45	1.55	0.11	1.7	2.13	-0.227	0.338	0.619	14.7	-6.86	9.48	1.05

Table IV. Baseline SKA2 survey specifications from [31] as in the Aggressive case in [25].

$z$	$V$	$n_g$	$b_g$	$s_B$	$s_F$	$\beta_B$	$\beta_F$	$\alpha_B$	$\alpha_F$	$\tau_1$	$B$
0.25	1.2	121.	0.674	0.371	-0.162	0.563	3.8	-2.14	-11.9	47.3	1.
0.35	2.1	71.8	0.73	0.442	-0.132	0.573	3.06	-0.891	-8.05	26.6	1.25
0.45	3.09	43.6	0.79	0.525	-0.126	0.576	2.56	-0.121	-6.07	17.5	1.49
0.55	4.11	26.8	0.854	0.607	-0.125	0.573	2.19	0.32	-4.77	12.2	1.72
0.65	5.11	17.	0.922	0.682	-0.121	0.565	1.9	0.535	-3.82	8.91	1.95
0.75	6.06	10.9	0.996	0.755	-0.118	0.554	1.67	0.641	-3.09	6.63	2.19

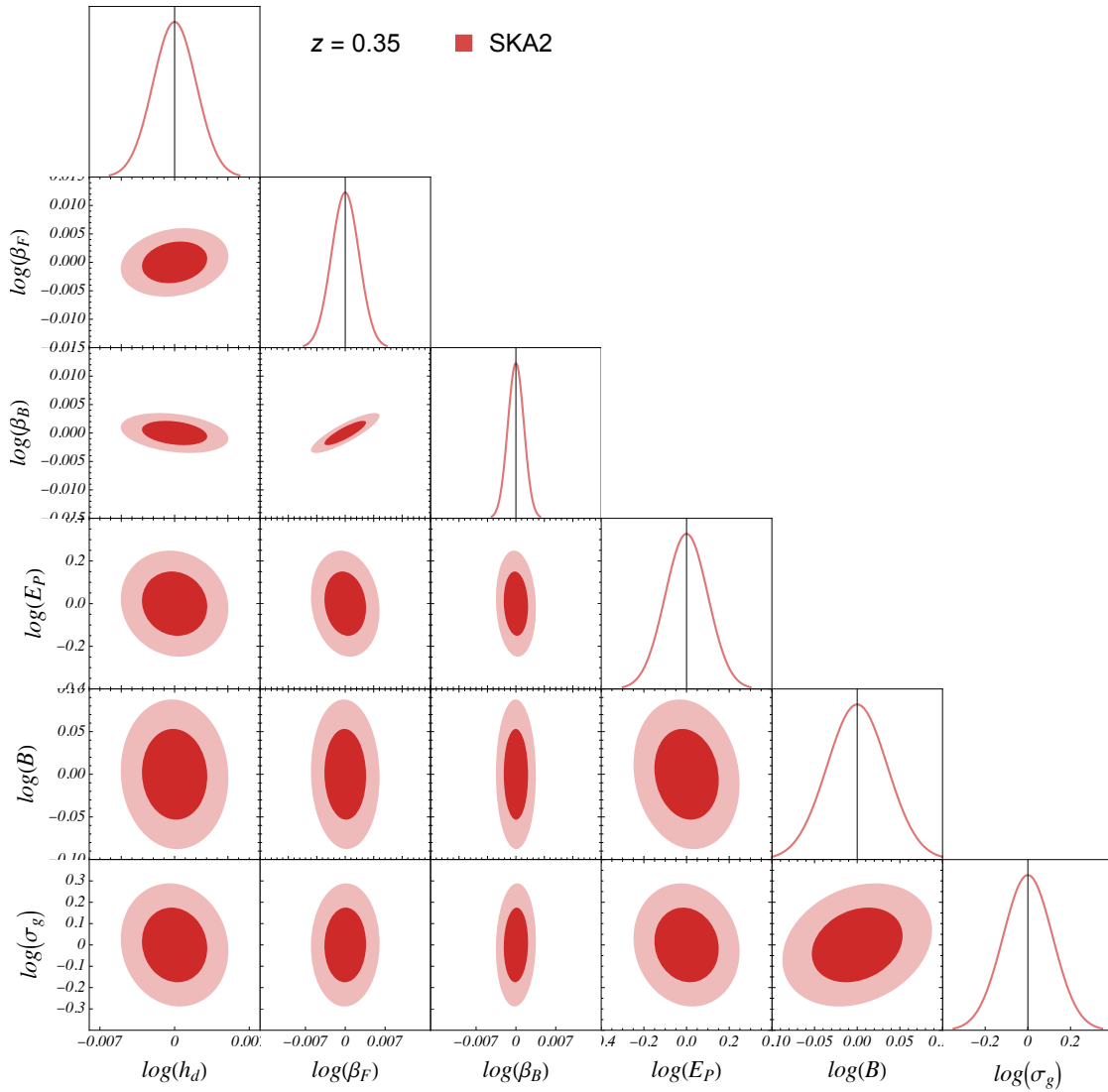


Figure 2. Corner plot for the baseline SKA2 survey at  $z = 0.35$  with one- and two-sigma regions. Since we always quote relative errors, the contour regions refer to the log of the parameters and, for each parameter  $\theta$ , are centered on  $\theta/\theta_{\text{fid}}$ .

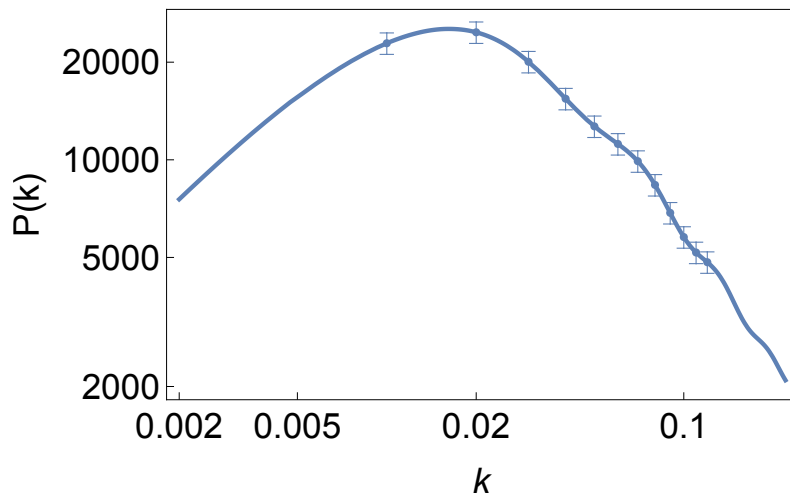


Figure 3. Fiducial linear power spectrum at present time and error bars for the baseline SKA2 survey.

- 
- [1] M. Moresco *et al.*, “Unveiling the Universe with emerging cosmological probes,” *Living Rev. Rel.*, vol. 25, no. 1, p. 6, 2022.
- [2] Euclid Collaboration, “Cosmology and fundamental physics with the Euclid satellite,” *Living Rev. Rel.*, vol. 21, no. 1, p. 2, 2018.
- [3] G. W. Horndeski, “Second-order scalar-tensor field equations in a four-dimensional space,” *Int. J. Theor. Phys.*, vol. 10, pp. 363–384, 1974.
- [4] M. Ishak *et al.*, “Modified Gravity Constraints from the Full Shape Modeling of Clustering Measurements from DESI 2024,” 11 2024.
- [5] C. Bonvin and P. Fleury, “Testing the equivalence principle on cosmological scales,” *JCAP*, vol. 05, p. 061, 2018.
- [6] C. Bonvin, F. O. Franco, and P. Fleury, “A null test of the equivalence principle using relativistic effects in galaxy surveys,” *JCAP*, vol. 08, p. 004, 2020.
- [7] S. Castello, N. Grimm, and C. Bonvin, “Rescuing constraints on modified gravity using gravitational redshift in large-scale structure,” *Phys. Rev. D*, vol. 106, no. 8, p. 083511, 2022.
- [8] C. Bonvin and L. Pogosian, “Modified Einstein versus modified Euler for dark matter,” *Nature Astron.*, vol. 7, no. 9, pp. 1127–1134, 2023.
- [9] S. Castello, Z. Wang, L. Dam, C. Bonvin, and L. Pogosian, “Disentangling modified gravity from a dark force with gravitational redshift,” *Phys. Rev. D*, vol. 110, no. 10, p. 103523, 2024.
- [10] L. Amendola, “Linear and non-linear perturbations in dark energy models,” *Phys. Rev. D*, vol. 69, p. 103524, 2004.
- [11] S. Castello, M. Mancarella, N. Grimm, D. S. Blanco, I. Tutusaus, and C. Bonvin, “Gravitational Redshift Constraints on the Effective Theory of Interacting Dark Energy,” *JCAP*, vol. 05, p. 003, 2024.
- [12] L. Amendola, “Coupled quintessence,” *Phys. Rev. D*, vol. 62, p. 043511, 2000.
- [13] C. Bonvin and R. Durrer, “What galaxy surveys really measure,” *Phys. Rev. D*, vol. 84, p. 063505, 2011.
- [14] A. Challinor and A. Lewis, “The linear power spectrum of observed source number counts,” *Phys. Rev. D*, vol. 84, p. 043516, 2011.
- [15] J. Yoo, A. L. Fitzpatrick, and M. Zaldarriaga, “A New Perspective on Galaxy Clustering as a Cosmological Probe: General Relativistic Effects,” *Phys. Rev. D*, vol. 80, p. 083514, 2009.
- [16] N. Kaiser, “Clustering in real space and in redshift space,” *Mon. Not. Roy. Astron. Soc.*, vol. 227, pp. 1–27, 1987.
- [17] eBOSS Collaboration, “Completed SDSS-IV extended Baryon Oscillation Spectroscopic Survey: Cosmological implications from two decades of spectroscopic surveys at the Apache Point Observatory,” *Phys. Rev. D*, vol. 103, no. 8, p. 083533, 2021.
- [18] G. Jelic-Cizmek, F. Lepori, C. Bonvin, and R. Durrer, “On the importance of lensing for galaxy clustering in photometric and spectroscopic surveys,” *JCAP*, vol. 04, p. 055, 2021.
- [19] F. Lepori *et al.*, “Euclid preparation - XIX. Impact of magnification on photometric galaxy clustering,” *Astron. Astrophys.*, vol. 662, p. A93, 2022.
- [20] V. Tansella, C. Bonvin, R. Durrer, B. Ghosh, and E. Sellentin, “The full-sky relativistic correlation function and power spectrum of galaxy number counts. Part I: theoretical aspects,” *JCAP*, vol. 03, p. 019, 2018.
- [21] P. McDonald, “Gravitational redshift and other redshift-space distortions of the imaginary part of the power spectrum,” *JCAP*, vol. 11, p. 026, 2009.
- [22] C. Bonvin, L. Hui, and E. Gaztanaga, “Asymmetric galaxy correlation functions,” *Phys. Rev. D*, vol. 89, no. 8, p. 083535, 2014.
- [23] M. Raveri, L. Pogosian, M. Martinelli, K. Koyama, A. Silvestri, and G.-B. Zhao, “Principal reconstructed modes of dark energy and gravity,” *JCAP*, vol. 02, p. 061, 2023.
- [24] F. Beutler and E. Di Dio, “Modeling relativistic contributions to the halo power spectrum dipole,” *JCAP*, vol. 07, no. 07, p. 048, 2020.
- [25] M. Quartin, L. Amendola, and B. Moraes, “The  $6 \times 2$ pt method: supernova velocities meet multiple tracers,” *Mon. Not. Roy. Astron. Soc.*, vol. 512, no. 2, pp. 2841–2853, 2022.
- [26] J. Koda, C. Blake, T. Davis, C. Magoulas, C. M. Springob, M. Scrimgeour, A. Johnson, G. B. Poole, and L. Staveley-Smith, “Are peculiar velocity surveys competitive as a cosmological probe?,” *Mon. Not. Roy. Astron. Soc.*, vol. 445, no. 4, pp. 4267–4286, 2014.
- [27] C. Howlett, A. S. G. Robotham, C. D. P. Lagos, and A. G. Kim, “Measuring the growth rate of structure with Type IA Supernovae from LSST,” *Astrophys. J.*, vol. 847, no. 2, p. 128, 2017.
- [28] H. Magira, Y. P. Jing, and Y. Suto, “Cosmological Redshift-Space Distortion on Clustering of High-Redshift Objects: Correction for Nonlinear Effects in the Power Spectrum and Tests with N-Body Simulations,” *Astrophys. J.*, vol. 528, pp. 30–50, Jan 2000.
- [29] A. G. Adame *et al.*, “DESI 2024 VI: Cosmological Constraints from the Measurements of Baryon Acoustic Oscillations,” 4 2024.
- [30] D. Brout *et al.*, “The Pantheon+ Analysis: Cosmological Constraints,” *Astrophys. J.*, vol. 938, no. 2, p. 110, 2022.
- [31] P. Bull, “Extending cosmological tests of General Relativity with the Square Kilometre Array,” *Astrophys. J.*, vol. 817, no. 1, p. 26, 2016.
- [32] A. Aghamousa *et al.*, “The DESI Experiment Part I: Science, Targeting, and Survey Design,” 10 2016.
- [33] C. Bonvin, F. Lepori, S. Schulz, I. Tutusaus, J. Adamek, and P. Fosalba, “A case study for measuring the relativistic dipole of a galaxy cross-correlation with the Dark Energy Spectroscopic Instrument,” *Mon. Not. Roy. Astron. Soc.*, vol. 525, no. 3, pp. 4611–4627, 2023.
- [34] E. Paillas, Y.-C. Cai, N. Padilla, and A. G. Sánchez, “Redshift-space distortions with split densities,” *Mon. Not. Roy.*



- Astron. Soc.*, vol. 505, no. 4, pp. 5731–5752, 2021.
- [35] Planck Collaboration VI, “Planck 2018 results. VI. Cosmological parameters,” *Astron. Astrophys.*, vol. 641, p. A6, 2020. [Erratum: *Astron.Astrophys.* 652, C4 (2021)].
- [36] S. Yahya, P. Bull, M. G. Santos, M. Silva, R. Maartens, P. Okouma, and B. Bassett, “Cosmological performance of SKA HI galaxy surveys,” *Mon. Not. Roy. Astron. Soc.*, vol. 450, no. 3, pp. 2251–2260, 2015.
- [37] S. Camera, M. G. Santos, and R. Maartens, “Probing primordial non-Gaussianity with SKA galaxy redshift surveys: a fully relativistic analysis,” *Mon. Not. Roy. Astron. Soc.*, vol. 448, no. 2, pp. 1035–1043, 2015. [Erratum: *Mon.Not.Roy.Astron.Soc.* 467, 1505–1506 (2017)].